ISSN 1674-1056
http://cpb.iphy.ac.cn
http://iopscience.iop.org/cpb
中国物理 B
Chinese Physics
中国物理
Chinese Physics B

# Real-time frequency transfer system over ground-to-satellite link based on carrier-phase compensation at $10^{-16}$ level

Hui-Jian Liang(梁慧剑), Shi-Guang Wang(王时光), Yu Bai(白钰), Si-Chen Sun(孙思忱), and Li-Jun Wang(王力军)
**Citation:**Chin. Phys. B, 2021, 30 (**8**): 080601. DOI: 10.1088/1674-1056/ac05a6
Journal homepage: http://cpb.iphy.ac.cn; http://iopscience.iop.org/cpb

**What follows is a list of articles you may be interested in**

---

## Evaluation of second-order Zeeman frequency shift in NTSC-F2

Jun-Ru Shi(施俊如), Xin-Liang Wang(王心亮), Yang Bai(白杨), Fan Yang(杨帆), Yong Guan(管勇), Dan-Dan Liu(刘丹丹), Jun Ruan(阮军), and Shou-Gang Zhang(张首刚)
Chin. Phys. B, 2021, 30 (**7**): 070601. DOI: 10.1088/1674-1056/abe375

## Improvement of the short-term stability of atomic fountain clock with state preparation by two-laser optical pumping

Lei Han(韩蕾), Fang Fang(房芳), Wei-Liang Chen(陈伟亮), Kun Liu(刘昆), Shao-Yang Dai(戴少阳), Ya-Ni Zuo(左娅妮), and Tian-Chu Li(李天初)
Chin. Phys. B, 2021, 30 (**5**): 050602. DOI: 10.1088/1674-1056/abe22a

## Study of optical clocks based on ultracold $^{171}$Yb atoms

Di Ai(艾迪), Hao Qiao(谯皓), Shuang Zhang(张爽), Li-Meng Luo(骆莉梦), Chang-Yue Sun(孙常越), Sheng Zhang(张胜), Cheng-Quan Peng(彭成权), Qi-Chao Qi(齐启超), Tao-Yun Jin(金涛韫), Min Zhou(周敏), Xin-Ye Xu(徐信业)
Chin. Phys. B, 2020, 29 (**9**): 090601. DOI: 10.1088/1674-1056/aba099

## A transportable optical lattice clock at the National Time Service Center

De-Huan Kong(孔德欢), Zhi-Hui Wang(王志辉), Feng Guo(郭峰), Qiang Zhang(张强), Xiao-Tong Lu(卢晓同), Ye-Bing Wang(王叶兵), Hong Chang(常宏)
Chin. Phys. B, 2020, 29 (**7**): 070602. DOI: 10.1088/1674-1056/ab9290

## Fiber-based joint time and frequency dissemination via star-shaped commercial telecommunication network

Yi-Bo Yuan(袁一博), Bo Wang(王波), Li-Jun Wang(王力军)
Chin. Phys. B, 2017, 26 (**8**): 080601. DOI: 10.1088/1674-1056/26/8/080601

---

# Real-time frequency transfer system over ground-to-satellite link based on carrier-phase compensation at $10^{-16}$ level*

Hui-Jian Liang(梁慧剑)[1,2], Shi-Guang Wang(王时光)[2,3,†], Yu Bai(白钰)[2,3], Si-Chen Sun(孙思忱)[2,3], and Li-Jun Wang(王力军)[1,2,3,4,‡]

[1] *Department of Electronic Engineering, Tsinghua University, Beijing* 100084, *China*
[2] *State Key Laboratory of Precision Measurement Technology and Instruments, Tsinghua University, Beijing* 100084, *China*
[3] *Department of Precision Instruments, Tsinghua University, Beijing* 100084, *China*
[4] *Department of Physics, Tsinghua University, Beijing* 100084, *China*

(Received 6 April 2021; revised manuscript received 20 May 2021; accepted manuscript online 27 May 2021)

We demonstrate a novel and stable frequency transfer scheme over ground-to-satellite link based on real-time carrier-phase detection and compensation. We performed a zero-baseline measurement with the designed system, an uninterrupted frequency standard signal is recovered in the reception station without additional post-correction of delay error caused in the route, which is because the phase error of the entire route is tracked and compensated continuously in real-time. To achieve this goal, we employed two carriers in the system and the differential signal is transferred in order to eliminate the instability results from the local oscillator at the satellite transponder as well as the common-mode noise induced in the transfer route and microwave components. The stability of $3 \times 10^{-16}$ with an integration time of 1 day was achieved and the time fluctuation during one day was measured to be about $\pm 20$ ps. Error sources and possible solutions are discussed. Our zero-baseline method shows a promising result for real-time satellite-based time and frequency transfer and deserves further research to find whether it works between long-baseline stations.

**Keywords:** frequency transfer, ground-to-satellite link, carrier-phase compensation

**PACS:** 06.30.Ft, 07.50.–e, 06.20.fb **DOI:** 10.1088/1674-1056/ac05a6

## 1. Introduction

Modern high-performance optical atomic clocks have surpassed the best cesium clocks that are used to define the second in the International System of Units (SI) by at least two orders of magnitude in terms of accuracy and stability.[1–4] These best measuring devices are essential in numerous applications such as accurate time and frequency dissemination, relativistic geodesy, quantum secure, astronomy, searches for dark matter, and verification of basic physical theories (Lorentz symmetry, Einstein equivalence principle, and time variation of fundamental constants).[5–12] To exploit the full potential of these atomic clocks, ultra-stable frequency transfer methods with lowest degradation are in eager demand.[13,14] Tremendous progress has been achieved in time-frequency transfer over optical-fiber-based links. Methods that enable optical atomic clock comparisons with a fractional uncertainty below $10^{-20}$ are developed[15,16] and frequency transfer experiments in remote distance are successfully conducted over dark-fiber and dark-wavelength links.[17,18] Various applications require frequency transfer via free space links. A recent carrier-phase (CP) optical two-way time-frequency transfer (OTWTFT) experiment reaches frequency comparisons with a fractional stability of $1.2 \times 10^{-17}$ at 1-s averaging time over a turbulent 4-km free space link.[19]

Satellite-based time and frequency transfer by microwave signals is indispensable to compare remote atomic clocks because it is challenging and costly to construct intercontinental fiber links. Two conventional techniques are engaged to form the timescale network of Coordinated Universal Time (UTC) and International Atomic Time (TAI) established between Bureau International des Poids et Mesures (BIPM) and timing institutions around the world.[20] The first technique utilizes signals (in the L band) from global navigation satellite systems (GNSSs), such as the US Global Positioning System (GPS), the European Galileo, the Russian GLONASS, or the Chinese Beidou. The measurement precision by GPS L1 Coarse/Acquisition (C/A) code with common view method is about 5 ns in 13 min for time transfer[21] and GPS P3 gets results less than 1 ns.[22] By detecting the carrier-phase of the GPS signal, precise point positioning (PPP) and integer PPP (IPPP) methods improved the frequency comparison precision to several tens of picoseconds and an instability of $10^{-15}$ level is reached with an averaging time of 1 day.[23,24] The second technique with higher accuracy is two-way satellite time and frequency transfer (TWSTFT) via geostationary satellites, which typically employs a pseudo-random-noise (PRN) code

*Project supported by the National Key Research and Development Program of China (Grant No. 2016YFA0302101) and the Initiative Program of State Key Laboratory of Precision Measurement Technology and Instruments.

†Corresponding author. E-mail: wangsg@tsinghua.edu.cn
‡Corresponding author. E-mail: lwan@tsinghua.edu.cn

© 2021 Chinese Physical Society and IOP Publishing Ltd 

at the rate of 2.5-Mega chips per second (Mcps). This method achieves transfer accuracy less than a nanosecond and uncertainty at $10^{-15}$ level within an integration time of 1 day.[25] Modulated signal with higher chip rate leads to better measurement precision as well as wider bandwidth occupation in satellite transponder, which means more lease costs and limit the performance. To exploit further improvements, the carrier-phase-based TWSTFT technique provided a much developed measurement instability of $2\times10^{-13}$ at 1 s and the long-term instability reached the $10^{-16}$ level.[26,27] A comparison experiment of Sr and Yb optical lattice clocks by this method has been operated.[28] A GPU-based two-way time transfer modem with dual pseudo-random-noise (DPN) code has been developed and the results are consistent with GPS carrier-phase methods.[29] Common-view methods (GNSS-based techniques) engage the timing signals received from the satellites at the same time, estimate and correct the phase delay error from satellite to receiver before exchange the detected time differences between distant institutions. Two-way methods (TWSTFT techniques) exchange the timing signals via satellite simultaneously. Although timing signals are transferred between the two ground stations in both directions, the transmission is not completely symmetric. The time delay differences derived from ionospheric, tropospheric and satellite transponder in two directions also need to be corrected after the reception. In both cases, correction for time delays (or time delay differences) are conducted after the reception of timing signals. This process relies on extra data such as regional vertical total electron content (TEC) maps, mathematical atmosphere model and affects the measurement precision. Consequently, these two methods output post-corrected timing signals point-by-point with certain time intervals.

As comparison, frequency transfer with real-time carrier-phase measurement and compensation is free from the post-processing and an uninterrupted stable frequency standard signal can be recovered in the remote site. Synchronization experiments between a ground station and Quasi-Zenith Satellite System (QZSS) onboard oscillators using navigation signals as feedback control have been reported, the stability of $1.23\times10^{-14}$ at 100160 s is obtained.[30] A real-time frequency dissemination link based on active carrier-phase compensation has been constructed, reaching the relative stability of $3.2\times10^{-13}/\mathrm{s}$ and $4.4\times10^{-17}/\mathrm{d}$ over 80-m free space.[31,32] In previous work, we engaged a microwave link between one ground station and the satellite to detect the carrier-phase noise in real-time.[33] After compensation, the result of remaining phase error calculated by the host computer is recorded as the result but no frequency standard signal been recovered in the ground station. In this article, we achieve the aim to transfer a real analog frequency standard signal between two ground stations via the satellite. Compared with previous work, the experimental system is carefully redesigned, we employed a customized two-channel signal-generator to get ultra-stable transmitted carrier signal. We also engaged designed frequency down-converters to ensure best phase coherence and get promising performance. A continuous and stable frequency standard signal is recovered in the specialized recovery module of reception station. The remaining time fluctuation error for actual frequency standard signal transfer of this system evaluated with 15 days measurement is about $\pm20$ ps, which is 10 times better than the digital phase noise detection result of $\pm200$ ps in previous work during 3 days. In this paper, we introduce the equations and scheme of our carrier-phase-based method in Section 2 and describe the experimental setup in Section 3. In Section 4, the results and error sources are discussed.

## 2. Scheme of carrier-phase-based frequency transfer

As depicted in Fig. 1, the total scheme consists of two ground stations and one geostationary earth orbit (GEO) satellite, note that three microwave links connect the whole system. Initially, we want to explain how a single signal propagates in the scheme. In link 1, ground station A transmits a signal and receives its own re-transmitted signal from the satellite. The phase of the transmitted signal is represented as

$$\phi_{\mathrm{A}} = \omega_{\mathrm{A}}t + \varphi_{\mathrm{A0}}, \tag{1}$$

where $\omega_{\mathrm{A}}$ represents the angular frequency and $\varphi_{\mathrm{A0}}$ is the initial phase. The transmitted signal suffers phase delays induced by turbulent atmosphere in uplink and downlink which are expressed as $\varphi_{\mathrm{Au}}$ and $\varphi_{\mathrm{Ad}}$, respectively. Satellite transponder introduces translation phase fluctuation denoted as $\varphi_{\mathrm{S}}$. Ground station A conducts a phase compensation $\Delta\varphi_{\mathrm{A}}$ to the transmitted signal before it is sent out. Hence, the phase information at the satellite $\phi_{\mathrm{S}}$ and received by station A $\phi'_{\mathrm{A}}$ are respectively expressed as

$$\phi_{\mathrm{S}} = \phi_{\mathrm{A}} + \Delta\varphi_{\mathrm{A}} + \varphi_{\mathrm{Au}} + \varphi_{\mathrm{S}}, \tag{2}$$

$$\phi'_{\mathrm{A}} = \phi_{\mathrm{S}} + \varphi_{\mathrm{Ad}} = \phi_{\mathrm{A}} + \Delta\varphi_{\mathrm{A}} + \varphi_{\mathrm{Au}} + \varphi_{\mathrm{S}} + \varphi_{\mathrm{Ad}}. \tag{3}$$

Ground station B observes the phase of both its own re-transmitted signal and that from the counterpart station A via the satellite. Link 2 is the round-trip microwave link between station B and the satellite where there is no compensation module as station A. The phases of the transmitted and received signal in link 2 are written as

$$\phi_{\mathrm{B}} = \omega_{\mathrm{B}}t + \varphi_{\mathrm{B0}}, \tag{4}$$

$$\phi'_{\mathrm{B}} = \phi_{\mathrm{B}} + \varphi_{\mathrm{Bu}} + \varphi_{\mathrm{S}} + \varphi_{\mathrm{Bd}}. \tag{5}$$

The phase delay information accumulated in link 2 can be distinguished by comparing Eqs. (4) and (5).

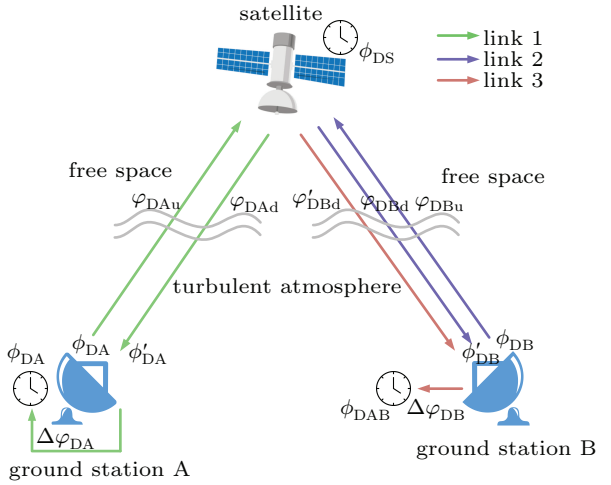



**Fig. 1.** Total scheme of carrier-phase-based frequency transfer. Each link consists of two carrier signals that propagate simultaneously and the differential signal is transmitted. Consequently, phase fluctuation introduced by the satellite is cancelled.

The uplink of link 3 is the same with that of link 1, and the downlink is the link in which station B observes signal from station A via the satellite. After signal reception in station B, there is a phase shifter for compensation. The phase of compensated signal is expressed as

$$\phi_{AB} = \phi_S + \varphi'_{Bd} + \Delta\varphi_B, \tag{6}$$

here $\varphi'_{Bd}$ is the phase delay caused in downlink 3 and $\Delta\varphi_B$ represents the phase compensated by the phase shifter.

When

$$\Delta\varphi_A = -(\varphi_{Au} + \varphi_S), \tag{7}$$
$$\Delta\varphi_B = -\varphi'_{Bd}, \tag{8}$$

according to Eqs. (2) and (6),

$$\phi_{AB} = \phi_S = \phi_A. \tag{9}$$

We can see that the frequency standard signal in station A is recovered in station B by links 1 and 3. Link 2 operates to detect $\Delta\varphi_B$ since $\varphi'_{Bd}$ is proportional to $\varphi_{Bd}$ with their corresponding frequency in the downlink. $\varphi_S$ at the satellite is indispensable to determine the value of $\Delta\varphi_A$ and $\Delta\varphi_B$. However, it is unknown and far away from measurement instruments to detect. Besides, the observation of single reception carrier signal in ground station shows a fierce phase fluctuation, which makes it hard to meet the high compensation rate demands. Therefore, we promote the scheme by engaging two carrier frequencies simultaneously in each link instead of just one. The differential signal of the two carriers is transmitted actually. Consequently, $\varphi_S$ is canceled by phase subtraction between two carriers. Additionally, the phase noises induced to each carrier in one same link are common-mode noises, which are positively correlated since two carriers transmit via an identical microwave channel simultaneously. As a result, the differential signal phase fluctuates much smoother than one single carrier and can be measured and compensated precisely in real-time. After the cancelation of $\varphi_S$, $\varphi_{Au}$ and $\varphi'_{Bd}$ can be distinguished by dividing the whole phase delay proportionally with their corresponding up and down frequencies in link 1 and link 2, respectively.

In the promoted two-carrier scheme, the phase of the transmitted and received differential signal in link 1 and link 2 are respectively expressed as follows (as shown in Fig. 1):

$$\phi_{DA} = \omega_{DA}t + \varphi_{DA0}, \tag{10}$$
$$\phi'_{DA} = \phi_{DA} + \Delta\varphi_{DA} + \varphi_{DAu} + \varphi_{DAd}, \tag{11}$$
$$\phi_{DB} = \omega_{DB}t + \varphi_{DB0}, \tag{12}$$
$$\phi'_{DB} = \phi_{DB} + \varphi_{DBu} + \varphi_{DBd}. \tag{13}$$

Here, $\omega_{Di}$ ($i$ = A or B) is the frequency gap between the two carriers in station $i$, $\varphi_{Di0}$ ($i$ = A or B) is the initial phase difference. $\Delta\varphi_{DA}$ represents the phase compensated to the differential signal before sent in station A. $\varphi_{Dij}$ ($i$ = A or B, $j$ = u or d) is the phase delay of $j$ link between station $i$ and the satellite. Hence, the phase information at the satellite $\phi_{DS}$ and that received in link 3 $\phi_{DAB}$ are given by

$$\phi_{DS} = \phi_{DA} + \Delta\varphi_{DA} + \varphi_{DAu}, \tag{14}$$
$$\phi_{DAB} = \phi_{DS} + \varphi'_{DBd} + \Delta\varphi_{DB}, \tag{15}$$

where $\Delta\varphi_{DB}$ is the phase compensated to the reception differential signal in station B.

When

$$\Delta\varphi_{DA} = -\varphi_{DAu}, \tag{16}$$
$$\Delta\varphi_{DB} = -\varphi'_{DBd}, \tag{17}$$

a frequency standard signal transmitted from station A is received at station B, since $\phi_{DAB} = \phi_{DS} = \phi_{DA}$ according to Eqs. (14) and (15). $\Delta\varphi_{DA}$ and $\Delta\varphi_{DB}$ can be estimated by comparing Eqs. (10), (11), and (12), (13) to get the whole phase delay in link 1 and link 2 and then proportionally divide them with corresponding up and down frequencies in the link.

The total scheme of frequency transfer is to some extend complex. Three ground-to-satellite transmission links are required and each link consists of two microwave channels. Besides, the signal processing modules dealing with multi-signal from satellite are complicated. Therefore, we believe it is necessary to build a simplified zero-baseline frequency transfer system before extending it to operate over long-baseline. More importantly, we can figure out whether the scheme deserves extension for practical use by evaluating the transfer precision of zero-baseline.

The zero-baseline system shares the same two-carrier mechanism. Two ground stations are located together, consequently, the three pairs uplinks and downlinks in the total scheme overlap to be the one same pair, as depicted in Fig. 2.

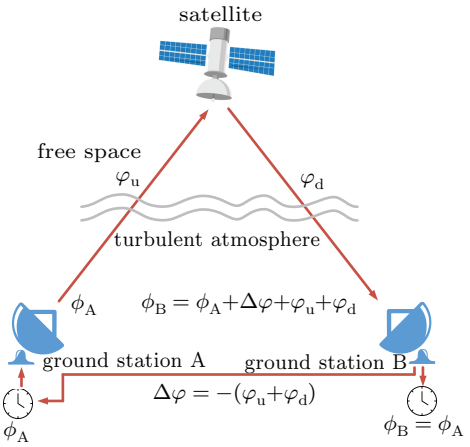



**Fig. 2.** Scheme of zero-baseline frequency transfer system. The frequency standard signal is disseminated from ground station A to station B. The link consists of two carrier signals.

The phase of the received signal is denoted as

$$\phi_B = \phi_A + \Delta\varphi + \varphi_u + \varphi_d, \tag{18}$$

here, $\phi_A$ represents the phase of the transmitted signal, $\Delta\varphi$ is the compensated phase, $\varphi_u$ and $\varphi_d$ represent phase noise in uplink and downlink, respectively. If the phase delay of the entire route $\varphi_r$ (uplink plus downlink) is compensated, which makes

$$\Delta\varphi = -\varphi_r = -(\varphi_u + \varphi_d), \tag{19}$$

as a result, the frequency standard signal is disseminated from station A to station B. By comparing signals of reception and transmission, the transfer accuracy and stability of the designed system can be detected.

## 3. Experimental setup of carrier-phase-based frequency transfer system

A frequency transfer experiment was performed over zero-baseline to evaluate transmission performance. Two ground stations A and B were co-located in the State Key Laboratory of Precision Measurement Technology and Instruments, Tsinghua University in Beijing as transmitter and receiver. We employed two Ku band carriers with a frequency gap of 120 MHz. Figure 3 depicts the configuration of the experimental system.

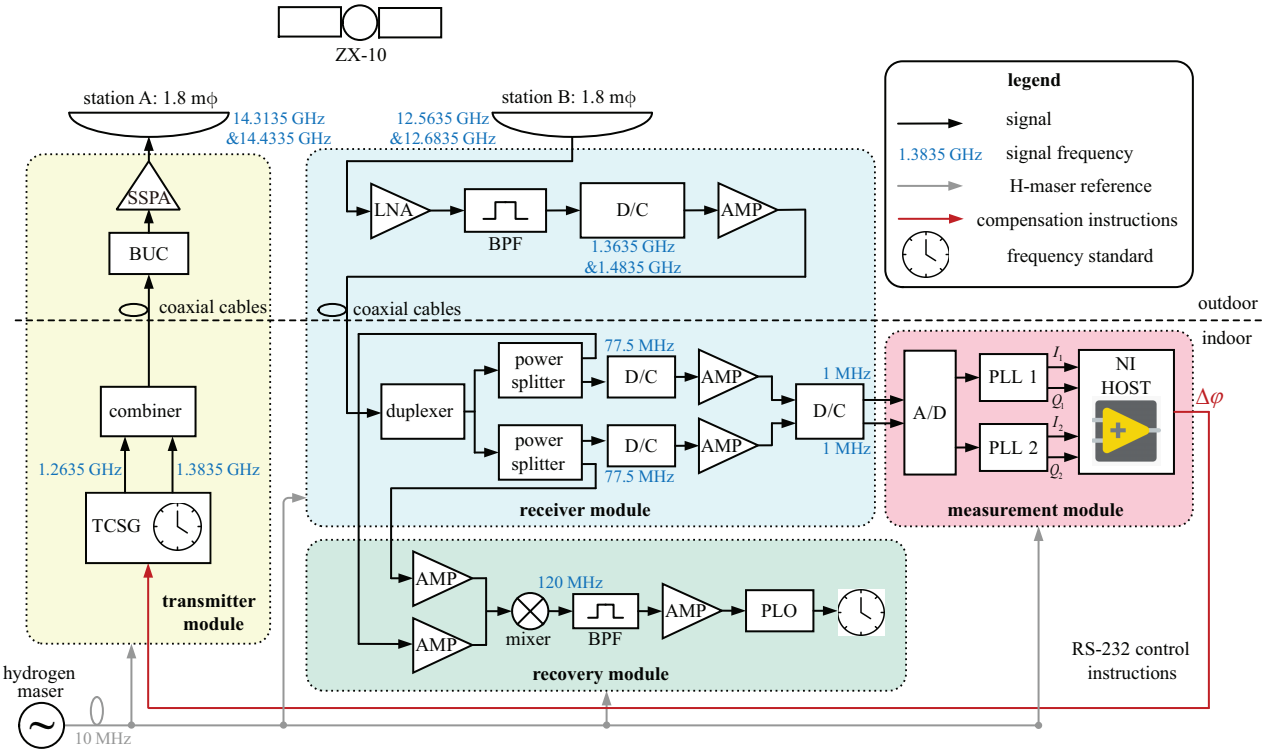



**Fig. 3.** Configuration of the experimental system for carrier-phase-based frequency transfer. TCSG: two-channel signal-generator, BUC: block-up-converter, SSPA: solid-state power amplifier, LNA: low-noise amplifier, BPF: band-pass filter, D/C: frequency down-converter, AMP: amplifier, A/D: analog-to-digital sampler, PLL: phase-locked-loop, PLO: phase-locked-oscillator.

### 3.1. Transmission ground station A

In the transmission ground station A, we employed a two-channel signal-generator (TCSG) to generate two single frequency signals with 1.2635 GHz and 1.3835 GHz, which was phase-locked to the external 10-MHz hydrogen maser. The two signals were combined together by a signal combiner, and then up-converted to carrier frequencies at 14.3135 GHz and 14.4335 GHz using a commercially block-up-converter (BUC). The combined carrier signals were amplified by a solid-state power amplifier (SSPA) and fed to a 1.8-m ring-focus dish antenna. The antenna was equipped on the rooftop and the elevation angle was 43.3°. The frequency parame-

ters are listed in Table 1. We customized the TCSG to make its output signals adjustable with phase and power. Hence, phase compensation was conducted by controlling TCSG, and the power of each carrier was balanced to avoid power-interference between the carriers transmitted simultaneously. Table 2 shows the parameters of the customized TCSG.

**Table 1.** Frequency parameters of each carrier link.

| | Frequency parameters | Carrier link 1 | Carrier link 2 |
|---|---|---|---|
| Transmission station A | TCSG (GHz) | 1.2635 | 1.3835 |
| | uplink (GHz) | 14.3135 | 14.4335 |
| Reception station B | downlink (GHz) | 12.5635 | 12.6835 |
| | cable transmission (GHz) | 1.3635 | 1.4835 |
| | intermediate frequency (MHz) | 77.5 | 77.5 |
| | signal processing (MHz) | 1 | 1 |
| | recovered signal (MHz) | 120 | |

**Table 2.** Parameters of customized TCSG.

| Parameters | Value |
|---|---|
| Centre frequency (GHz) | 1.2635 & 1.3835 |
| Adjustable bandwidth for each channel (MHz) | ±5 |
| Reference frequency (MHz) | 100 |
| Frequency adjustable resolution (Hz) | $1 \times 10^{-6}$ |
| Phase adjustable resolution (°) | 0.03 |
| Power adjustable resolution (dBm) | 0.1 |
| Control interface | RS-232 |
| Instruction response time (ms) | $< 0.05$ |

### 3.2. GEO satellite transponder

The transponder employed was one commercial communication GEO satellite ZX-10 located at a longitude of 110.5° east. The satellite works as a conventional frequency down-converter with an onboard oscillator. We rented two channels with bandwidth of 1 MHz for each to conduct the experiment. Parameters of ZX-10 are shown in Table 3.

**Table 3.** Parameters of ZX-10.

| Parameters | Value |
|---|---|
| Orbit slot (°E) | 110.5 |
| Orbit precision (°) | ±0.5 |
| Polarization | linear |
| Ku bandwidth (GHz) | 14.00–14.50/12.25–12.75 |
| Number of Ku transponder | 16 |
| Bandwidth of Ku transponder (MHz) | 30 & 36 |
| Frequency conversion stability | $\pm 7 \times 10^{-7}$ (day)<br>$\pm 1 \times 10^{-6}$ (month) |

### 3.3. Reception ground station B

The reception ground station B consisted of three functional modules, including receiver module, measurement module and recovery module. The antenna installed in station B was identical to that in station A. In the receiver module, the carriers at 12.5635 GHz and 12.6835 GHz were amplified by a low-noise amplifier (LNA) and passed through a 200-MHz bandwidth band-pass filter (BPF). Then, they were down-converted to lower 1.3635 GHz and 1.4835 GHz signals using a frequency down-converter (D/C) and amplified by an additional amplifier, by which the carrier signals were suitable for a 50-m long transmission in coaxial cable link from outdoor rooftop to indoor laboratory. The two carriers were separated with a duplexer and split into two pairs of signals by two splitters, one pair of signals were set as inputs to the recovery module, and the other pair were down-converted to the intermediate-frequency (IF) 77.5-MHz signals by two D/Cs, respectively. The pair of IF signals passed through one extra two-channel D/C to become 1 MHz in frequency, which were input into the phase measurement module. Table 1 shows the specific frequency parameters. All the frequency conversions were carried out by converters assembled as depicted in Fig. 4. The reference signal of 10 MHz from one hydrogen maser was provided to all converters to maintain the carrier-phase coherence. We engaged a 60-m coaxial cable link and a high-performance-distribution-amplifier (HPDA) to distribute 10-MHz reference signal because of that the ground station was located away from the laboratory where hydrogen maser was operated. However, we confirmed that the distribution instability was negligible compared to the stability of the original reference signal which is at about $10^{-15}$ level for averaging times exceeding $10^4$ s.

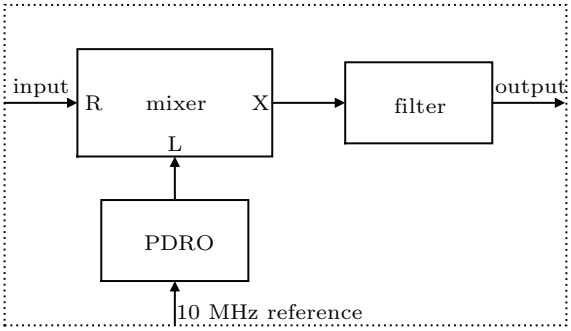



**Fig. 4.** Setup of frequency converters in the experiment. Local site of the mixer was supplied by a phase-locked dielectric-resonator-oscillator (PDRO) with 10-MHz reference from the hydrogen maser.

The measurement module was dedicated for detecting the carrier-phase of two received carriers in order to calculate the entire phase delay of the differential signal, which is given as $\varphi_r$ in Eq. (19). We employed the National Instrument (NI) product NI-5782 as a two-channel analog-to-digital (A/D) sampler to deal with the pair of 1-MHz signals. Data sampling was performed with a sampling rate of 50 MHz in synchronized timing with the external 10-MHz reference signal. An NI-7976 field-programmable gate array (FPGA) board was connected to the A/D sampler for signal processing. Two sampled data sequences of the two carriers were filtered by digital BPFs and send to phase-locked-loops (PLLs) in parallel. Two PLLs reshaped the received signals by canceling the power variation and eliminating extra phase noise whose frequency

is out of the phase locking bandwidth. The PLLs designed in FPGA were Costas loops, whose outputs include both in-phase (I) and quadrature (Q) components. Two digitalized IQ data sequences were written to an NI-8135 host computer by an FPGA-to-HOST first-input-first-output (FIFO) register every 20 ms. Each data package contained 1024 continuously sampled points for each PLL. We used LabVIEW in the host computer to perform further calculation. For data from each PLL (index $k$ is used to distinguish them), in spite of signal amplitude, the original received signal and the phase-locked I/Q branches were expressed as $S_k$, $S_{Ik}$, and $S_{Qk}$ ($k = 1$ or 2),

$$S_k = \sin(\phi_{ik}), \tag{20}$$

$$S_{Ik} = \sin(\phi_{pk}), \tag{21}$$

$$S_{Qk} = \cos(\phi_{pk}), \tag{22}$$

$\phi_{ik}$ and $\phi_{pk}$ ($k = 1$ or 2) represent the original input phase and the locked phase of corresponding PLL. The phase tracking error $\varphi_{epk}$ can be computed by a complex operation with an arg calculation to extract the phase of a complex number,

$$\begin{aligned} \varphi_{epk} &= \mathrm{Arg}(S_k \cdot S_{Ik} - \mathrm{i} \cdot (S_k \cdot S_{Qk})) \\ &\approx \mathrm{Arg}(\mathrm{e}^{\mathrm{i}(\phi_{ik} - \phi_{pk})}) = \phi_{ik} - \phi_{pk}. \end{aligned} \tag{23}$$

This error signal indicates the tracking ability of PLL. Another complex calculation was performed to get the entire phase delay of the differential signal $\varphi_r$ which equals the phase difference of the two reception carriers,

$$\begin{aligned} \varphi_r &= \mathrm{Arg}((S_{Q1} + \mathrm{i} \cdot S_{I1}) \cdot ((S_{Q2} - \mathrm{i} \cdot S_{I2})) \\ &= \mathrm{Arg}(\mathrm{e}^{\mathrm{i}(\phi_{p1} - \phi_{p2})}) = \phi_{p1} - \phi_{p2}. \end{aligned} \tag{24}$$

According to Eq. (19), the compensated phase $\Delta\varphi$ should be set as follows, and it is expected to be expressed with another form

$$\Delta\varphi = -\varphi_r = \omega_{doppler} t + \varphi_v, \tag{25}$$

where $\omega_{doppler}$ represents the Doppler shifts caused by the satellite motion and $\varphi_v$ is the remaining phase variation.

The schematic diagram of phase compensation strategy is depicted in Fig. 5. The process was initialized until two PLLs tracked tightly with received carriers respectively, which was distinguished by observing whether error signals $\varphi_{ep1}$ and $\varphi_{ep2}$ stay stable during 5-s data statistics. The compensation process consists of two parts, one part was the Doppler frequency which was evaluated by linear fitting the phase data, and the other part was the remaining phase variation which is calculated engaging a proportional-integral-differential (PID) controller. Doppler frequency compensation was performed once every 5 s, while phase compensation was conducted every 100 ms. The PID controller was enabled after the frequency compensation for the first time since frequency offset was sufficiently cancelled then. Corresponding control instructions were sent to the TCSG in the transmitter with given period.

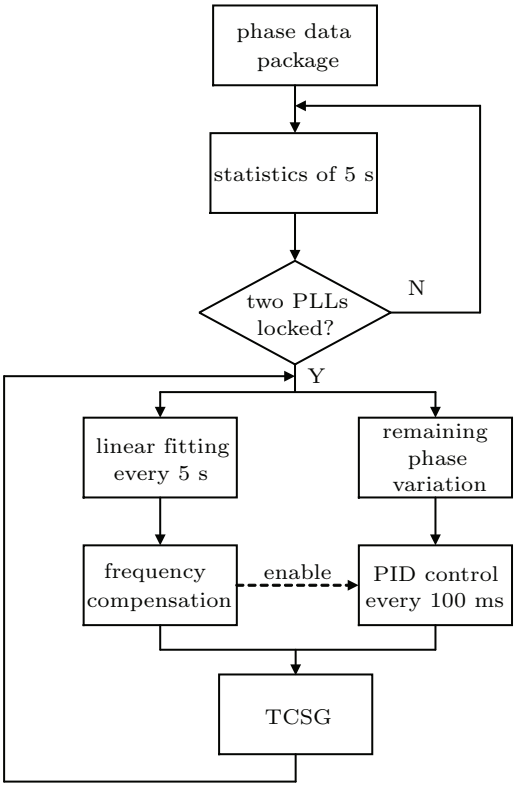



**Fig. 5.** Compensation strategy for received differential signal. Doppler frequency and remaining phase variation were compensated separately after initialization.

The recovery module was developed for real-time frequency standard signal reproduction. The other pair of carriers from splitters in the receiver module were amplified and mixed to get the differential signal which was 120 MHz with full-path phase fluctuation. The differential signal was filtered by a narrow-band filter with the bandwidth of 20 kHz and passed through an amplifier. Then, it was sent to a phase-locked-oscillator (PLO) as the reference signal for the purpose of signal reshape. When the measurement module operating in parallel, the entire propagation phase noise is continuously compensated to the transmitted signal, forming a PLL over ground-to-satellite link. Consequently, the phase of recovered signal from PLO is synchronized with the transmitted signal in real-time and the frequency standard signal is transferred.

## 4. Results and discussion

Figure 6 shows the phase fluctuation of the recovered differential signal. As indicated previously, the phase variation in the free running system (the black line) is consistent with the form in Eq. (25), where periodic fluctuation indicating the Doppler shift effect exists. In contrast, when the phase compensation has been engaged, the remaining phase error becomes tiny and stable (the red line).

In the case of the PLL over ground-to-satellite link was closed with phase compensation, we recorded the time fluctuation of the recovered signal from April 11, 2020 to April

26, 2020 (MJD 58950 to 58965) for over 15 days, as depicted in Fig. 7(a). Besides, the time fluctuation in MJD 58955 is measured by a histogram and a Gaussian fit is performed in Fig. 7(b), showing that the full width at half maximum (FWHM) of time fluctuation during one day is about ±20 ps.

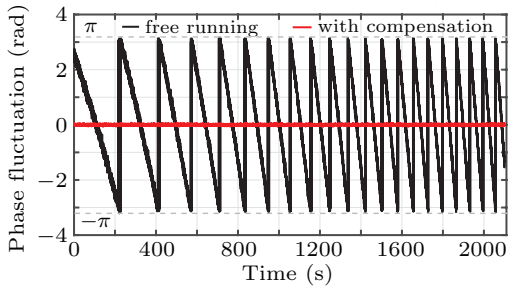



**Fig. 6.** Phase fluctuation of the recovered differential signal in free running system (the black line) and with compensation (the red line).

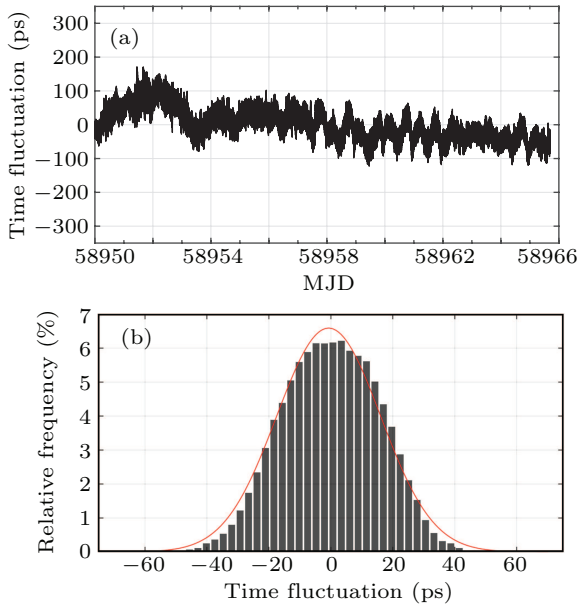



**Fig. 7.** Time fluctuation of the experiment with phase compensation. (a) Time fluctuation of the recovered signal from April 11, 2020 to April 26, 2020. (b) The histogram of time fluctuation in MJD 58955 with a Gaussian fit, FWHM = ±20 ps.

The frequency stability (modified Allan deviation) of the recovered signal over the same 15 days period is depicted with that of the transmitted differential signal in Fig. 8. Room temperature variations during daytime with a period of about 2300 s caused the bump at around 1000 s for both recovered and transmitted frequency stability. We plot the time fluctuation of the transmitted signal for about 4 days in Fig. 9 to show this variation. The data is recorded from 0:00 at day 1, the red line shows the time variation during daytime of day 1 (from 8:00 to 24:00) at an amplitude of about 25 ps, which is synchronized with diurnal temperature variation. The blue line (from 0:00 to 8:00 at day 2) shows a significantly more stable time fluctuation since the temperature varies slowly during night-time.

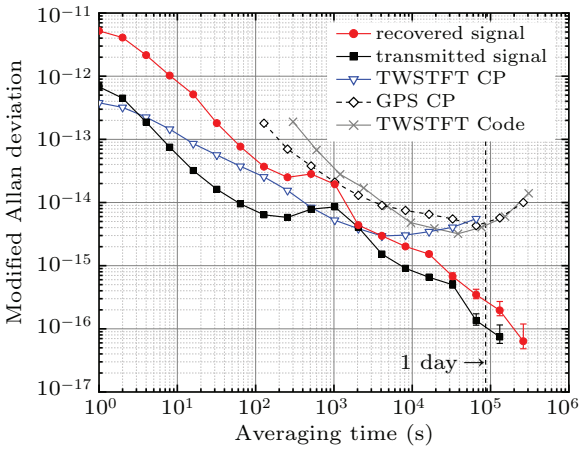



**Fig. 8.** Measured frequency stability of recovered signal and transmitted signal in our zero-baseline experiment. The frequency stability achieved over 150-km short-baseline by NICT with TWSTFT CP, GPS CP, and TWSTFT Code methods are also plotted.

In the total transfer scheme (see Fig. 1), the uplink noise from ground station A to satellite $\varphi_{\mathrm{DAu}}$ is calculated in link 1, similarly, the downlink noise from satellite to ground station B $\varphi_{\mathrm{DBd}}$ is calculated in link 2. The two links are site-dependent from each other. Link 3 requires $\varphi_{\mathrm{DAu}}$ (relies only on the observation of link 1) and $\varphi_{\mathrm{DBd}}$ (relies only on the observation of link 2) to transfer frequency standard from station A to station B. The setup of links 1 and 2 is similar with the zero-baseline experiment, so we can deduce that $\varphi_{\mathrm{DAu}}$ and $\varphi_{\mathrm{DBd}}$ are with the same stability level of zero-baseline result. So does the superposition of $\varphi_{\mathrm{DAu}}$ and $\varphi_{\mathrm{DBd}}$ in the operation of link 3. As a consequence, the performance of total scheme is expected to be with the same transfer level of zero-baseline experiment. In comparison, we depict the transmission stability of TWSTFT CP, GPS CP (with PPP), and TWSTFT Code in Fig. 8, respectively, which are achieved over 150-km short-baseline by National Institute of Information and Communications Technology (NICT).[26] The stability of the recovered signal in our experiment is limited by that of the transmitted signal over the whole range. It is clear from Fig. 8 that the transmission stability of our system is superior to that of GPS CP and TWSTFT Code. When the averaging time exceeds 100 s, our method is at the same level with TWSTFT CP, excluding the bump around several hundred seconds, with the temperature variations being the cause. The long-term stability of TWSTFT CP is limited by that of the hydrogen maser. Over an averaging time of 1 day, the stability reaches $3 \times 10^{-16}$ in our zero-baseline transmission.

The measurement floor of the PLLs engaged in our system is evaluated by directly sending signals from a signal generator into the measurement module. The average phase-locking error is less than 0.0001 rad, which corresponds to about 0.13-ps time jitter and is considered negligible. However, the PLL tracking ability degraded when tracking satellite signals which suffered considerable phase noise and significant signal-to-noise ratio (SNR) deterioration. The residual

phase-locking error is measure to be 0.01 rad for each PLL in the experiment, it is comparable to a time jitter of 13 ps. The tracking instability of two PLLs combined randomly in the measurement module, causing a total phase-locking error of approximately 18 ps, which is about $\sqrt{2}$ times the phase-locking error in each PLL.

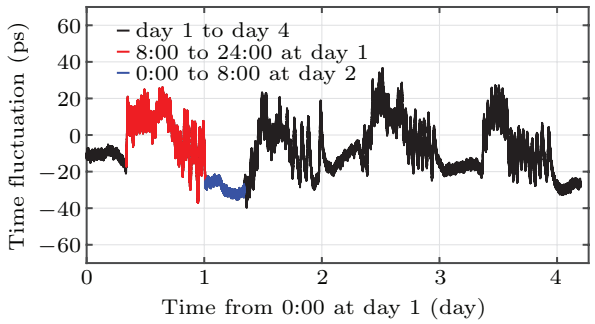



**Fig. 9.** Time fluctuation of the transmitted signal for about 4 days. The variation in daytime (the red line) is significantly larger than that during night-time (the blue line), indicating the effects caused by diurnal temperature variation.

Microwave components, especially those frequency converters and power amplifiers, contribute to measurement instability. Nevertheless, it should be noted that the two transmitted carriers in the experiment propagate throughout one same link with common components simultaneously. Consequently, the phase noise induced by these components are common-mode noises and can be significantly eliminated by phase subtraction in the recovered differential signal. The temperature variations affect not only indoor measurement as discussed before. During our experiment, we observed that the average transmission power out of SSPA (see Fig. 3) decreased by about 5 dB in daytime compared to that in night-time for which diurnal temperature variation is believed to be the cause. Temperature-stabilization is required for both indoor and outdoor equipments to attain better performance. The frequency gap between the two carriers occupied in our experiment is 120 MHz, according to the parameters of ZX-10 satellite listed in Table 3, we can deduce that the two carrier signals were not converted by the same transponder at the satellite. Hence, the difference of frequency response characteristic for the two corresponding transponders introduced extra phase noise to the measurement.

## 5. Conclusion

In summary, we demonstrate a novel and stable scheme of ground-to-satellite frequency transfer based on real-time carrier-phase compensation. Different from common-view and two-way methods, an uninterrupted analog frequency standard signal is recovered in the reception station without additional post-correction of delay error caused in the route, which is because the phase error of the entire route is tracked and compensated continuously in real-time. We employed two carriers in the system and the differential signal is transferred actually in order to eliminate the instability results from the local oscillator at the satellite transponder as well as the common-mode noise induced in the transfer route and microwave components. Consequently, the differential signal phase fluctuates much smoother than one single carrier and can be measured and compensated precisely in real-time.

In the verification zero-baseline measurement over 15 days, the FWHM of time fluctuation during one day was obtained to be approximately $\pm 20$ ps and the modified Allan deviation of the recovered signal reached about $3 \times 10^{-16}$ with an averaging time of 1 day. It can be seen that the transmission stability of our system is superior to that of GPS CP and TW-STFT Code. Major factors that limited the measurement precision were discussed, developing PLLs with superior tracking ability and temperature-stabilization are believed to be the most effective ways to take full advantage of our scheme. Our experiment shows a promising precision for real-time satellite-based time and frequency transfer. In future work, we are going to extend the zero-baseline scheme to the total scheme as shown in Fig. 1. This method can be applied in various applications including atomic clock comparison, positioning and navigation, and metrology researches.

## References

[1] Schioppo M, Brown R C, McGrew W F, Hinkley N, Fasano R J, Beloy K, Yoon T H, Milani G, Nicolodi D, Sherman J A, Phillips N B, Oates C W and Ludlow A D 2017 *Nat. Photon.* **11** 48
[2] Ushijima I, Takamoto M, Das M, Ohkubo T and Katori H 2015 *Nat. Photon.* **9** 185
[3] Huntemann N, Sanner C, Lipphardt B, Tamm C and Peik E 2015 *Phys. Rev. Lett.* **116** 063001
[4] Hinkley N, Sherman J A, Phillips N B, Schioppo M, Lemke N D, Beloy K, Pizzocaro M, Oates C W and Ludlow A D 2015 *Science* **341** 1215
[5] Matveev A, Parthey C G, Predehl K, Alnis J, Beyer A, Holzwarth R, Udem T, Wilken T, Kolachevsky N, Abgrall M, Rovera D, Salomon C, Laurent P, Grosche G, Terra O, Legero T, Schnatz H, Weyers S, Altschul B and Hänsch T W 2013 *Phys. Rev. Lett.* **110** 230801
[6] Lisdat C, Grosche G, Quintin N *et al.* 2016 *Nat. Commun.* **7** 1
[7] Dai H, Shen Q, Wang C Z, Li S L, Liu W Y, Cai W Q, Liao S K, Ren J G, Yin J, Chen Y A, Zhang Q, Xu F H, Peng C Z and Pan J W 2020 *Nat. Phys.* **16** 848
[8] Arzoumanian Z, Brazier A, Burke-Spolaor S, *et al.* 2015 *The Astrophysical Journal* **813** 65
[9] Derevianko A and Pospelov M 2015 *Nat. Phys.* **10** 933
[10] Dzuba V A, Flambaum V V, Safronova M S, Porsev S G, Pruttivarasin T, Hohensee M A, and Häffner H 2016 *Nat. Phys.* **12** 465
[11] Altschul B, Bailey Q G, Blanchet L *et al.* 2015 *Advances in Space Research* **55** 501
[12] Godun R M, Nisbet-Jones P B R, Jones J M, King S A, Johnson L A M, Margolis H S, Szymaniec K, Lea S N, Bongs K and Gill P 2014 *Phys. Rev. Lett.* **113** 210801
[13] Riehle F 2017 *Nat. Photon.* **11** 25
[14] Levine J 2008 *Metrologia* **45** S162
[15] Raupach S M F, Koczwara A and Grosche G 2015 *Phys. Rev. A* **92** 021801
[16] Bercy A, Stefani F, Lopez O, Chardonnet C, Pottie P-E and Amy-Klein A 2014 *Phys. Rev. A* **90** 061802
[17] Droste S, Ozimek F, Udem T, Predehl K, Hänsch T W, Schnatz H, Grosche G and Holzwarth R 2013 *Phys. Rev. Lett.* **111** 110801
[18] Lisdat C, Grosche G, Quintin N *et al.* 2016 *Nat. Commun.* **7** 1
[19] Sinclair L C, Bergeron H, Swann W C, Baumann E, Deschênes J D and Newbury N R 2018 *Phys. Rev. Lett.* **120** 050801
[20] Panfilo G and Arias E F 2009 *IEEE Transactions on Ultrasonics, Ferroelectrics and Frequency Control* **57** 140

[21] Lewandowski W, Petit G and Thomas C 1993 *IEEE Transactions on Instrumentation and Measurement* **42** 474
[22] Bauch A, Achkar J, Bize S, Calonico D, Dach R, Hlavać R, Lorini L, Parker T, Petit G, Piester D, Szymaniec K and Uhrich P 2005 *Metrologia* **43** 109
[23] Droste S, Grebing C, Leute J, Raupach S M F, Matveev A, Hänsch T W, Bauch A, Holzwarth R and Grosche G 2015 *New Journal of Physics* **17** 083044
[24] Petit G, Kanj A, Loyer S, Delporte J, Mercier F and Perosanz F 2015 *Metrologia* **52** 301
[25] Piester D, Bauch A, Becker J, Staliuniene E and Schlunegger C 2008 *IEEE Transactions on Ultrasonics, Ferroelectrics and Frequency Control* **55** 1906
[26] Fujieda M, Gotoh T, Nakagawa F, Tabuchi R, Aida M and Amagai J 2012 *IEEE Transactions on Ultrasonics, Ferroelectrics and Frequency Control* **59** 2625
[27] Fujieda M, Piester D, Gotoh T, Becker J, Aida M and Bauch A 2014 *Metrologia* **51** 253
[28] Fujieda M, Yang S-H, Gotoh T, Hwang S-W, Hachisu H, Kim H, Lee Y K, Tabuchi R, Ido T, Lee W-K, Heo M-S, Park C Y, Yu D-H and Petit G 2018 *IEEE Transactions on Ultrasonics, Ferroelectrics and Frequency Control* **65** 973
[29] Gotoh T, Amagai J, Hobiger T, Fujieda M and Aida M 2010 *IEEE Transactions on Instrumentation and Measurement* **60** 2495
[30] Iwata T, Matsuzawa T, Machita K and Abei A 2011 *International Journal of Navigation and Observation* **2011** 849814
[31] Miao J, Wang B, Gao C, Bai Y, Zhu X and Wang L J 2013 *Review of Scientific Instruments* **84** 104703
[32] Miao J, Wang B, Bai Y, Yuan Y B, Gao C and Wang L J 2015 *Review of Scientific Instruments* **86** 054704
[33] Sun S C, Bai Y, Liang H J, Wang S G and Wang L J 2019 *Review of Scientific Instruments* **90** 114708